2013 IEEE/RSJ International Conference on
Intelligent Robots and Systems (IROS)
November 3-7, 2013. Tokyo, Japan

Fully-Autonomous Coordinated Flight of Multiple UAVs using Decentralized Virtual Leader Approach

Yoko Watanabe, Alexandre Amiez and Paul Chavent[1]

Abstract— **This paper presents experimental results of fully-autonomous coordinated flight of multiple UAVs. The coordination control law is designed based on the decentralized virtual leader approach, and its stability is theoretically proven. A mission scenario is defined by a sequence of four different coordination phases, to every of which the same controller is applied with different configuration settings. The proposed law has been implemented and demonstrated onboard the ONERA fixed-wing UAV platforms.**

I. INTRODUCTION

Coordinated operation of multiple unmanned aerial vehicles (UAVs) has aroused many researchers' interest in recent years, due to its great potential for increases in overall mission performance and robustness without augmenting a capacity of each UAV unit. For example, Acevedo et al. propose a cooperative long duration area surveillance system [1]. Hauert et al. suggest applying swarming UAVs to establish a communication network in rescue mission [2]. One should also refer to the impressive experimental work at GRASP Lab., who succeeded in flying up to twenty quadrotors in formation [3]. In these works, the coordination problem is rather treated at path planning level than at flight control level. Last year, ONERA has launched a research project to study in low-altitude aerial surveillance system using passive radar sensors distributed by a team of UAVs. For an efficient fusion of radar measurements, UAVs are required to fly in a precise formation during the mission. This project is our motivation to realize a coordination controller for multiple UAVs.

Various control strategies for multi-agent coordination have been investigated since many years. Especially, formation control has been intensively studied [4]. Formation control problem has two objectives. One is to form a desired geometric configuration, and the other is to achieve a mission. Two main approaches for such formation control are i) Leader-Follower (LF) approach and ii) Virtual Structure (VS) approach. In the LF approach, an agent designated as a leader takes charge of the global mission while the other agents designated as followers maintain a desired configuration with respect to the leader. An advantage of this approach lies in its facility of implementation, as no feedback loop from followers to the leader is needed. This is why most of the existing work on closed-loop UAV formation flight adopt the LF approach [5][6]. A drawback is its weak robustness to the leader's motion. Once losing the leader's performance, its error is fully propagated to all the followers and both the mission and coordination objectives can fail.

In order to overcome this robustness issue, the VS approach was introduced by [7]. VS is defined as a collection of agents, who maintains a desired geometric configuration. The approach consists of the following three steps; 1) VS is aligned with the current agent positions; 2) mission control is applied to VS to obtain a desired trajectory for each agent; and 3) each agent tracks its own desired trajectory. The mission and coordination objectives are both managed by a centralized VS control system with a state feedback from every agent. However, it can be easily decentralized by duplicating the system on each agent. For its capability to maintain a highly precise formation, many propose the VS approach for spacecraft or satellite formation control [8]. Only few applies it to multi-UAV control due to its high computational complexity of the VS alignment.

The virtual leader (VL) approach introduced by [9] is a combination of the two approaches discussed above. VL is determined from current states of every agent like a VS, then each agent maintains a desired configuration relative to the VL as followers do in the LF approach. Commonly the VL position is taken simply at a center of mass of all agents, and hence it does not require a complex optimization process. Moreover, the VL approach remains more robust than the LF approach because a failure of one agent will be only partially propagated to the others via the VL position. Since the VL approach overcomes the drawbacks of both the LF and the VS approaches, some propose its application to UAV formation flight [10] but not yet many examples of actual closed-loop UAV flight can be found.

This paper proposes a coordination controller for multiple UAVs based on the decentralized VL approach. Sepulchre et al. present a collective motion controller for a team of agents who have a 2D dynamics with a constant speed [11]. Their controller calculates heading rate input for each agent so that the agents converge on a circle orbit with a desired phase distribution. Inspired by this work, we design a controller for each UAV to achieve;

- a stable circle orbit around a VL position,
- a splay or synchronized phase distribution with the other agents on the circle, and
- a global mission objective.

Differences from the original work in [11] are that our agents have 2D control input (speed and heading rate), and that the circle center is controlled so that it coincides with a given VL position. The proposed controller can be applied to make different types of coordination by choosing different

[1] The authors are with Systems Control and Flight Dynamics Department, ONERA (The French Aerospace Laboratory), 31055 Toulouse, France. (First Name).(Last Name) at onera.fr

978-1-4673-6357-0/13/$31.00 ©2013 IEEE

Fig. 1. The ONERA ReSSAC Mousse UAV Platforms

configuration settings. For example, by taking a fixed beacon as a VL, UAVs can make a coordinated circling over a zone of interest. A formation flight can be attained by taking a VL in a conventional way, at a center of mass of the UAVs, with a zero circling speed. Another feature is that this controller is adaptive to any number of agents. This allows the system to handle easily an event of addition/deletion of an agent to/from the team even during operation.

The coordination controller designed in this paper has been implemented and tested onboard the ONERA fixed-wing UAV platforms (Figure 1). A mission scenario is defined by an automatic take-off phase followed by four different coordination phases. All of the coordination phases can be realized by the same controller, and transitions between them are executed by changing the controller settings. In experimental work of UAV closed-loop formation flight found in literature, it is often the case that a safety pilot manually places the follower UAV at a desired position relative to the leader before activating automatic formation [5][6]. Unlike those, we have achieved a fully-autonomous coordination flight of multiple UAVs without any manual adjustment. Flight test results are presented as a highlight of this paper.

II. COORDINATION CONTROLLER DESIGN

This section provides a coordination controller design and its stability analysis for different configurations.

A. (M, N)-Pattern Phase Distribution

Let $\boldsymbol{\theta} \in \mathbb{T}^N$ be a vector of N phase states where $\mathbb{T} = [0,\ 2\pi)$. Let $1 \le M \le N$ be a divisor of N. An (M, N)-pattern is a symmetric arrangement of N phases consisting of M clusters uniformly spaced around the unit circle, each with N/M synchronized phases. Then the (M, N)-potential function is defined by

$$U^{M,N}(\boldsymbol{\theta}) = \sum_{m=1}^{M} \frac{K_m}{2m^2N} \sum_{k=1}^{N}\sum_{j=1}^{N} \cos m(\theta_k - \theta_j) \quad (1)$$

Theorem 2.1: $\boldsymbol{\theta} \in \mathbb{T}^N$ is an (M, N)-pattern if and only if it is a global minimum of the potential function $U^{M,N}(\boldsymbol{\theta})$ with $K_m > 0$ for $m = 1, 2, ..., M-1$ and $K_M < 0$.

Proof: See *Theorem 6* in [11]. ■

Two special cases of (M, N)-pattern phase distribution are; i) synchronized state when $M = 1$ and ii) splay state when $M = N$. Figure 2 illustrates those two phase distributions in case of $N = 4$. This paper applies those states to multi-UAV coordination.

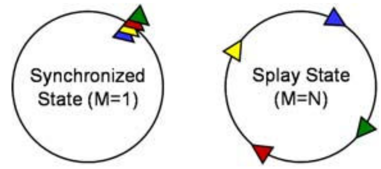

Fig. 2. Synchronized (left) and Splay (right) Phase Distribution

B. Coordination Controller with Known VL Trajectory

Let $\boldsymbol{X}_k$ $(k = 1, 2, \ldots, N)$ and $\boldsymbol{X}_{vl}$ be 2D position of the k-th agent and of a VL in an inertial reference frame. Define a relative position of the k-th agent to the VL by

$$\boldsymbol{r}_k = \boldsymbol{X}_k - \boldsymbol{X}_{vl} = r_k \begin{bmatrix} \cos\theta_k \\ \sin\theta_k \end{bmatrix} \quad (2)$$

where $r_k \ge 0$ and $\theta_k \in \mathbb{T}$ denote distance and phase. Define the system state $\boldsymbol{x}$ of the team of N agents by

$$\boldsymbol{x} = \begin{bmatrix} \boldsymbol{r}^T & \dot{\boldsymbol{r}}^T & \boldsymbol{\theta}^T & \dot{\boldsymbol{\theta}}^T \end{bmatrix}^T$$

where $\boldsymbol{r} = \begin{bmatrix} r_1 & \cdots & r_N \end{bmatrix}^T$ and $\boldsymbol{\theta} = \begin{bmatrix} \theta_1 & \cdots & \theta_N \end{bmatrix}^T$.

Theorem 2.2: Given a VL trajectory. With the control law (3) for each agent, every agent's trajectory converges to a circle orbit around the VL trajectory with a radius r_0, an angular velocity ω_0 and a phase configuration in a critical set of $U^{M,N}(\boldsymbol{\theta})$.

$$\ddot{\boldsymbol{X}}_k = u_{rk} \begin{bmatrix} \cos\theta_k \\ \sin\theta_k \end{bmatrix} + u_{\theta k} \begin{bmatrix} -\sin\theta_k \\ \cos\theta_k \end{bmatrix} + \ddot{\boldsymbol{X}}_{vl} \quad (3)$$

where

$$\begin{aligned} u_{rk} &= -K_r(r_k - r_0) - K_{\dot{r}}\dot{r}_k - K_{r\theta} r_k(\dot{\theta}_k - \omega_0)^2 - r_k\dot{\theta}_k^2 \\ u_{\theta k} &= -\frac{1}{r_k}\left(K_\theta \frac{\partial U^{M,N}(\boldsymbol{\theta})}{\partial \theta_k} + K_{\dot{\theta}}(\dot{\theta}_k - \omega_0)\right) \\ &\quad -(1 - K_{r\theta})\dot{r}_k(\dot{\theta}_k - \omega_0) + 2\dot{r}_k\dot{\theta}_k \end{aligned}$$

with positive gains. Furthermore, the splay and synchronized states are locally asymptotically stable (*l.a.s.*) when $M = N$ and $M = 1$, respectively.

Proof: The closed-loop dynamic system of the state $\boldsymbol{x}$ has the following limit cycle.

$$\begin{cases} r_k = r_0, \quad \dot{r}_k = 0, \quad \dot{\theta}_k = \omega_0 \quad \forall\ k \in \{1, 2, ..., N\} \\ \boldsymbol{\theta} \text{ of an } (M, N)\text{-pattern phase distribution} \end{cases} \quad (4)$$

Define a potential function as below.

$$\begin{aligned} V^{M,N}(\boldsymbol{x}) &= U^{M,N}(\boldsymbol{\theta}) + \frac{1}{2K_\theta}\sum_{k=1}^{N}\Big\{K_r(r_k - r_0)^2 + \\ &\quad \dot{r}_k^2 + r_k^2(\dot{\theta}_k - \omega_0)^2\Big\} \end{aligned} \quad (5)$$

This function is lower-bounded by $K_M N/2M^2$, which is attained uniquely at the limit cycle (4). A time derivative of this potential function is derived as

$$\dot{V}^{M,N}(\boldsymbol{x}) = -\frac{K_{\dot{r}}}{K_\theta}\sum_{k=1}^{N}\dot{r}_k^2 - \frac{K_{\dot{\theta}}}{K_\theta}\sum_{k=1}^{N}(\dot{\theta}_k - \omega_0)^2 \le 0 \quad (6)$$

In result, $V^{M,N}(\boldsymbol{x})$ is a Lyapunov function and the limit cycle (4) is stable. Let $\mathcal{S}$ be a set of all points in the state domain where $\dot{V}^{M,N}(\boldsymbol{x}) = 0$. Then, the largest invariant set in $\mathcal{S}$ can be given by

$$\mathcal{M} = \left\{ \boldsymbol{x} \in \mathcal{S} \mid r_k = r_0, \frac{\partial U^{M,N}(\boldsymbol{\theta})}{\partial \theta_k} = 0 \text{ for } \forall k \right\}$$

From LaSalle's invariant set theorem [12], every trajectory approaches to the invariant set $\mathcal{M}$.

Asymptotical stability of the splay and synchronized state can be proven by using Lyapunov indirect method. Let $\delta \boldsymbol{x}$ be a small disturbance from a state in the limit cycle (4). Then its dynamics can be linearized as below.

$$\begin{aligned} \delta \dot{\boldsymbol{x}} &= F(\boldsymbol{\theta}^*)\delta \boldsymbol{x} \\ &= \begin{bmatrix} O & I & O & O \\ -K_r I & -K_{\dot{r}} I & O & O \\ O & O & O & I \\ O & O & -\frac{K_\theta}{r_0^2} A(\boldsymbol{\theta}^*) & -\frac{K_{\dot{\theta}}}{r_0^2} I \end{bmatrix} \delta \boldsymbol{x} \end{aligned} \quad (7)$$

where $A(\boldsymbol{\theta}^*)$ is a Hessian matrix of the potential $U^{M,N}(\boldsymbol{\theta})$. All the eigenvalues of the matrix $F(\boldsymbol{\theta}^*)$ in (7) have a strictly negative real part, except the zero eigenvalue which corresponds to a steady rotation within the same limit cycle. Therefore, the splay and synchronized states are *l.a.s.* when $M = N$ and $M = 1$ respectively. ■

C. Coordination Controller with VL at Center of Mass

In formation control, it is common to take a VL at a center of mass of the agents, i.e., at

$$\boldsymbol{X}_{vl} = \frac{1}{N} \sum_{j=1}^{N} \boldsymbol{X}_j \quad (8)$$

Theorem 2.3: Define VL position by (8) and suppose a controller $\ddot{\boldsymbol{X}}_{vl} = \boldsymbol{u}_d$ gives a desired VL motion. With the control law (9) for each agent, the limit cycle (4) with the desired VL motion is stable.

$$\ddot{\boldsymbol{X}}_k = u_{rk} \begin{bmatrix} \cos\theta_k \\ \sin\theta_k \end{bmatrix} + u_{\theta k} \begin{bmatrix} -\sin\theta_k \\ \cos\theta_k \end{bmatrix} + \boldsymbol{u}_d \quad (9)$$

Furthermore, the splay state is *l.a.s.* when $M = N$.

Proof: Since $\ddot{\boldsymbol{X}}_{vl} = \boldsymbol{u}_d$ when $u_{rk} = u_{\theta k} = 0$ for $\forall\ k$, the closed-loop dynamics of $\boldsymbol{x}$ has the limit cycle (4). The potential function $V^{M,N}(\boldsymbol{x})$ in (5) still has its unique minimum at this limit cycle. Its time derivative becomes

$$\begin{aligned} \dot{V}^{M,N}(\boldsymbol{x}) &= -\frac{K_{\dot{r}}}{K_\theta} \sum_{k=1}^{N} \dot{r}_k^2 - \frac{K_{\dot{\theta}}}{K_\theta} \sum_{k=1}^{N} (\dot{\theta}_k - \omega_o)^2 \\ &+ \frac{1}{K_\theta} \left(\sum_{k=1}^{N} \dot{\boldsymbol{r}}_k - \omega_o \sum_{k=1}^{N} r_k \begin{bmatrix} -\sin\theta_k \\ \cos\theta_k \end{bmatrix} \right)^T (\boldsymbol{u}_d - \ddot{\boldsymbol{X}}_{vl}) \end{aligned}$$

From the definitions (2) and (8), the last term of the equation above vanishes. Hence, the limit cycle (4) is stable.

Consider the case of $M = N$. The linearized small disturbance dynamics about the splay state becomes

$$\delta \dot{\boldsymbol{x}} = G(\boldsymbol{\theta}^*)\delta \boldsymbol{x} = (F(\boldsymbol{\theta}^*) + \Delta G(\boldsymbol{\theta}^*))\, \delta \boldsymbol{x} \quad (10)$$

where

$$\Delta G(\boldsymbol{\theta}^*) = \begin{bmatrix} O & O & O & O \\ C_r & C_{\dot{r}} & C_\theta & C_{\dot{\theta}} \\ O & O & O & O \\ D_r & D_{\dot{r}} & D_\theta & D_{\dot{\theta}} \end{bmatrix}$$

The matrices C_* and D_* ($* = r, \dot{r}, \theta, \dot{\theta}$) can be given as a linear function of the matrices $\mathcal{C}$ and $\mathcal{S}$ whose (i,j)-elements are

$$\mathcal{C}_{ij} = \frac{1}{N} \cos\left((j-i)\frac{2\pi}{N} \right), \quad \mathcal{S}_{ij} = \frac{1}{N} \sin\left((j-i)\frac{2\pi}{N} \right)$$

All the eigenvalues of the matrix $G(\boldsymbol{\theta}^*)$ have a strictly negative real part except $\lambda = 0$ and $\lambda = \pm i\omega_0$. While the zero eigenvalue corresponds to a steady rotation, the eigenvalues $\lambda = \pm i\omega_0$ correspond to a translational shift of the limit cycle. It was not appeared in Theorem 2.2 because the VL motion was given. Hence, the splay state is proven to be *l.a.s.* when $M = N$. ■

D. Phase Constraint

In this subsection, a phase constraint is imposed on one of the agents so that its phase trajectory tracks a given reference.

Corollary 2.4: Let θ_d be a phase reference where $\dot{\theta}_d = \omega_0$. The controller (11) stabilizes the limit cycle (4) with a phase trajectory of the j-th agent converging to θ_d.

$$\ddot{\boldsymbol{X}}_k = u_{rk} \begin{bmatrix} \cos\theta_k \\ \sin\theta_k \end{bmatrix} + \tilde{u}_{\theta_k} \begin{bmatrix} -\sin\theta_k \\ \cos\theta_k \end{bmatrix} + \ddot{\boldsymbol{X}}_{vl} \quad (11)$$

where, with Kronecker delta δ_{jk},

$$\tilde{u}_{\theta_k} = u_{\theta k} - \frac{\delta_{jk}}{r_j} K_{\theta_d} \sin(\theta_j - \theta_d), \quad K_{\theta_d} > 0$$

Furthermore, the splay state is *l.a.s.* when $M = N$.

Proof: Define a new potential function by

$$W^{M,N}(\boldsymbol{x}) = V^{M,N}(\boldsymbol{x}) + \frac{K_{\theta_d}}{K_\theta} (1 - \cos(\theta_j - \theta_d)) \quad (12)$$

It attains its global minimum uniquely at the limit cycle (4) with $\theta_j = \theta_d$. Since $\dot{W}^{M,N}(\boldsymbol{x}) \le 0$, the phase-constrained limit cycle is stable. When $M = N$, the small disturbance dynamics can be linearized as

$$\delta \dot{\boldsymbol{x}} = \tilde{F}(\boldsymbol{\theta}^*)\delta \boldsymbol{x} = (F(\boldsymbol{\theta}^*) + \Delta F_j)\, \delta \boldsymbol{x} \quad (13)$$

where

$$\Delta F_j = -\frac{K_{\theta_d}}{r_0^2} \boldsymbol{e}_{(3N+j)} \boldsymbol{e}_{(2N+j)}^T$$

All the eigenvalues of $\tilde{F}(\boldsymbol{\theta}^*)$ have a strictly negative real part, and hence the splay state with $\theta_j = \theta_d$ is *l.a.s.* The zero eigenvalue of the matrix $F(\boldsymbol{\theta}^*)$ disappeared since the phase constraint will not allow the steady rotation. ■

Corollary 2.5: VL position is defined by (8). The controller (14) stabilizes the limit cycle (4) with $\theta_j = \theta_d$ and the VL motion following $\ddot{\boldsymbol{X}}_d = \boldsymbol{u}_d$.

$$\ddot{\boldsymbol{X}}_k = u_{rk} \begin{bmatrix} \cos\theta_k \\ \sin\theta_k \end{bmatrix} + \tilde{u}_{\theta_k} \begin{bmatrix} -\sin\theta_k \\ \cos\theta_k \end{bmatrix} + \boldsymbol{u}_d \quad (14)$$

Furthermore, the splay state is *l.a.s.* when $M = N$.

Proof: Similarly to the proofs of Theorem 2.3 and Corollary 2.4, $W^{M,N}(\boldsymbol{x})$ in (12) is a Lyapunov function and the limit cycle (4) with the phase constraint is stable. When $M = N$, the small disturbance dynamics is linearized about the phase-constrained splay state as

$$\delta\dot{\boldsymbol{x}} = \tilde{G}(\boldsymbol{\theta}^*)\delta\boldsymbol{x} = (G(\boldsymbol{\theta}^*) + \Delta G_j)\,\delta\boldsymbol{x} \tag{15}$$

where

$$\Delta G_j = \Delta F_j + \frac{K_{\theta_d}}{r_0^2}\begin{bmatrix} O & O & O & O \\ O & O & -\mathcal{S}\boldsymbol{e}_j\boldsymbol{e}_j^T & O \\ O & O & O & O \\ O & O & \mathcal{C}\boldsymbol{e}_j\boldsymbol{e}_j^T & O \end{bmatrix}$$

All the eigenvalues of $\bar{G}(\boldsymbol{\theta}^*)$ in (15) have a negative real part except $\lambda = \pm i\omega_0$ which correspond to a translational shift. Therefore, the splay state with $\theta_j = \theta_d$ is *l.a.s.* ■

More detailed proofs of the theorems and the corollaries above can be found in [13].

III. COORDINATED FLIGHT OF MULTIPLE UAVS

In this section, the coordination controller designed in Section II is applied to a mission of autonomous flight of multiple fixed-wing UAVs.

A. Mission Scenario

A global mission objective for a team of UAVs is to track a given sequence of waypoints in formation. A mission scenario from take-off to formation flight is defined by five different phases. The phases and their transition criteria are summarized below along with Figure 3.

- **Phase 0 - Take-off :** Given an entry point (*WP0*) of a waiting zone. UAV is launched at any timing and follows an automatic take-off procedure to reach *WP0* without any coordination with other UAVs.
- **Phase 1 - Wait :** If UAV reaches at *WP0*, it starts to make a circling motion around a fixed point $\boldsymbol{X}_c$ (determined from *WP0* and a radius *R0*) while forming a splay state (Figure 2-right) with UAVs who are already on this circle orbit.
- **Phase 2 - Transition :** Once all UAVs in the team are on standby in Phase 1, UAVs are commanded to make a transition from splay to synchronized state (Figure 2-left). This phase allows UAVs to get close each other before making a formation.
- **Phase 3 - Formation :** When all UAVs come close enough, they start to fly in formation with a formation distance $d0$ while the team still stays on the circle orbit.
- **Phase 4 - Mission :** As shown in Figure 3, a departing point $\boldsymbol{X}_d$ is identified on the circle orbit in function of a position of the first waypoint (*WP1*) relative to the circle. When the team of UAVs in formation reaches at $\boldsymbol{X}_d$, it departs for waypoint tracking mission (*WP1*→*WP2*→ $\cdots$) from the circle orbit.

Phases 1 through 4 can be realized by the coordination controller proposed in the previous section. A phase management function supervises current states of the team of UAVs and executes transitions simply by changing the controller settings according to Table I.

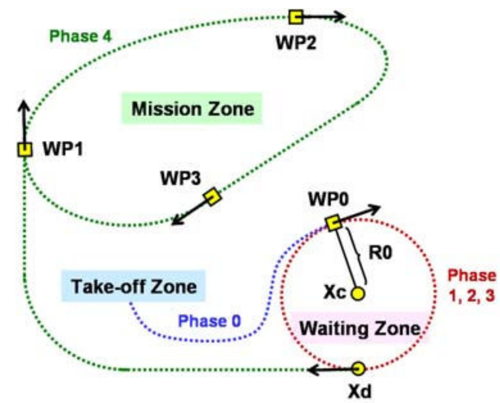

Fig. 3. Mission Scenario

TABLE I
COORDINATION CONTROLLER SETTINGS FOR EACH PHASE

Phase	1	2	3	4
Controller	Eqn. (3)		Eqn. (9) or (14)	
M	N (splay)	1 (synchro)	N (splay)	
r_0	circling radius : *R0*		formation radius : $d_0/2\sin(\pi/N)$	
ω_0	circling speed : *V0 / R0*		0	
VL	fixed-beacon : $\boldsymbol{X}_c$		center of mass : Eqn. (8)	
VL motion	no motion		circling	WP tracking

B. Decentralized Coordination Control System Architecture

The onboard control system architecture is designed based on the one already developed on our UAV platform for mono-use. The system consists of three components; i) mission management for flight mode and waypoint changes, ii) guidance law providing speed, heading and altitude commands to achieve a given flight mode/waypoint, and iii) flight controller which calculates actuator inputs from the guidance commands. The proposed coordination control system is incorporated in the guidance law component in a decentralized manner. That is, each UAV manages transitions of the coordination phases by its own, using the state information of other UAVs received via communication. This work assumes an ideal all-to-all communication and does not treat any problem associated with decentralization (incoherent decision, communication delay/failure, etc.). In this implementation, 2D acceleration input calculated in the coordination controller is converted to the horizontal velocity (speed+heading) command by integration. The nominal guidance laws for circling and waypoint tracking are used to obtain the desired VL motion ($\boldsymbol{u}_d$) in Phase 3 and 4. An anti-collision controller is also added to assure UAV flight safety. It is very important to have this anti-collision controller especially for Phase 2 during which UAVs try to get close each other. It is designed based on an artificial potential method, and is activated only when an UAV approaches to another UAV within a certain distance. The guidance commands for coordination and for anti-collision are combined before being sent to the flight controller.

C. 6 DoF Flight Simulation

The proposed coordination control system has been implemented in a 6 DoF flight simulator developed by ONERA/DCSD before its onboard implementation. The simulator includes a simple flight dynamics model of a fixed-wing aircraft, measurement models of onboard sensors, navigation filter for localization, and the three components of the flight control system. The coordination performance has been validated by realizing the entire mission scenario defined in III-A in this simulator.

IV. FLIGHT EXPERIMENT

This section first introduces our UAV experimental platforms and their hardware system, then presents results obtained in their successful coordination flight.

A. Experimental UAV Platform and Onboard Hardware

The ONERA ReSSAC Mousse fixed-wing UAV platforms shown in Figure 1 are developed based on the R/C airplane Multiplex Twinstar II, whose specifications are summarized in Table II. Figure 4 shows its onboard hardware system. The UAV is equipped with Xsens MTi IMU and μblox LEA-6H GPS for its self-localization. Two ARM7 micro processors are embedded; i) Processor CS (Switch Computer) is in charge of the radio command from a safety pilot, and ii) Processor CC (Control Computer) is dedicated to automatic flight control. The hardware includes a XBee wireless module which is used for communications with other UAVs and also with a ground control station (GCS). The onboard system architecture is illustrated in Figure 5. The software implementation on the processors CS and CC is done in C++ program. All functions in the flight control system run in sequence with a period of 50 (Hz). The guidance law component including the coordination controller is executed at 10 (Hz), whereas the wireless communication is updated only at 8.5 (Hz) due to its limited bandwidth.

TABLE II
SPECIFICATIONS OF THE RESSAC MOUSSE UAV

Empty weight	: 0.8 (kg)	Motor	: electric×2
Take-off weight	: 2 (kg)	Payload	: 0.5 (kg)
Fuselage length	: 1 (m)	Payload power supply	: 10 (W)
Wingspan	: 1.4 (m)	Flight duration	: 40 (min)

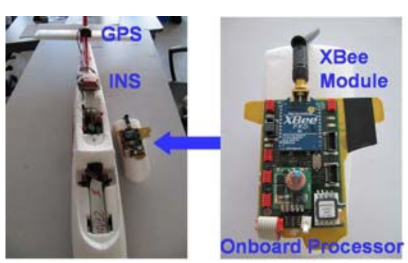

Fig. 4. Onboard Hardware of the ReSSAC Mousse UAV

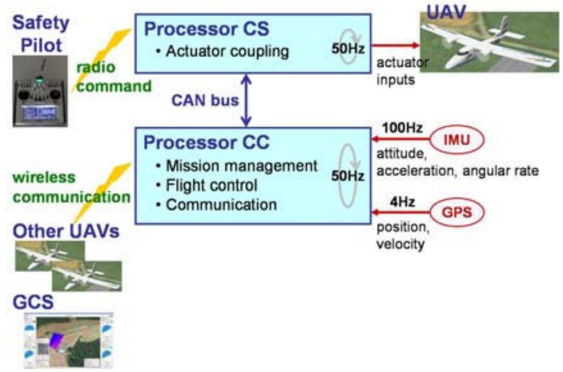

Fig. 5. Onboard System Architecture of the ReSSAC Mousse UAV

B. Results

Flight experiments have been conducted to perform the mission scenario defined in Section III-A by using the proposed coordination controller. After several preliminary tests, the implemented controller was simplified as listed below.

- In order to have smoother guidance commands, the following approximations were made on the inputs.

$$\begin{cases} u_{rk} \simeq -K_r\left(r_k - r_0\right) - K_{\dot r}\dot r_k - \|\dot{\boldsymbol{X}}_k\|\omega_0 \\ u_{\theta k} \simeq -\frac{1}{r_k}\left(K_\theta \frac{\partial U^{M,N}(\boldsymbol{\theta})}{\partial \theta_k} + K_{\dot\theta}(\dot\theta_k - \omega_0)\right) \end{cases}$$

- As the damping effects are already included in the low-level flight controller, we set up $K_{\dot\theta} = 0$ to have fast convergence on the phase distribution.

With this simplified version of the coordination controller, three ReSSAC Mousse UAVs have achieved a completely autonomous flight from Phase 0 (take-off) to Phase 4 (waypoint tracking in formation). A cut-off animation of this flight is illustrated in Figure 6, on which positions of the three UAVs, the VL and the waypoints are shown. The figures show the transitions of the coordination phases during the mission. First, two UAVs circled together over the waiting zone and then the third one joined them on the circle (two figures in the top row). Triggered by an operator on ground, the UAVs came close each other on the circle and made a formation (two figures in the middle row). Finally, they left for the mission of waypoint tracking while maintaining a formation (two figures in the bottom row). During the formation, a phase constraint was imposed so that one of the UAVs always locates at North of the VL. The control gains used in this test are;

$$K_r = 0.01V_0, \quad K_{dr} = 1.0, \quad K_\theta = K_{\theta_d} = 0.175$$

The circling radius and speed for the waiting phase were set as $R0 = 60$ (m) and $\omega_0 = 0.25$ (rad/sec), which gives the UAV nominal speed $V0 = 55$ (km/h). The formation distance between two UAVs was $d0 = 30$ (m). For security reason, they flew with an altitude difference of 20 (m). Figure 7 compares desired and real distances to the VL

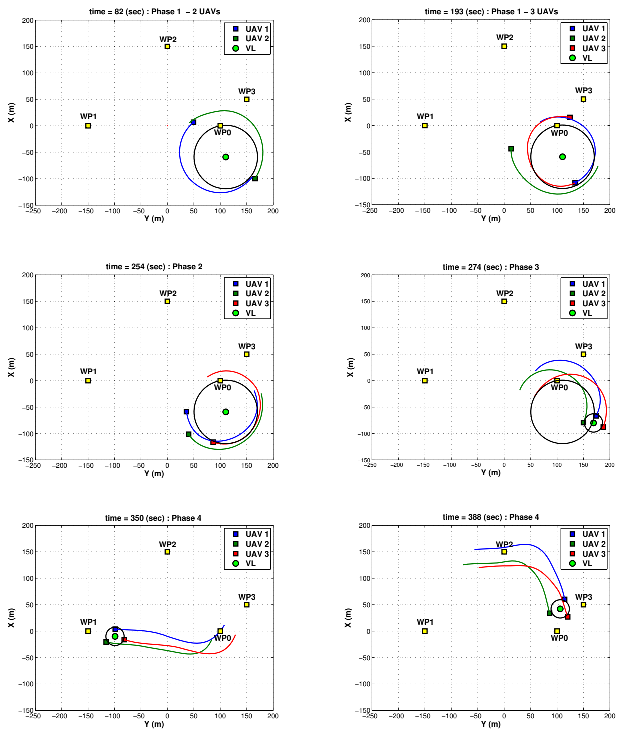

Fig. 6. Cut-off Animation of the Coordination Flight of Three UAVs

for each UAV. The precision of maintaining the formation distance is about ± 10 (m). Figure 8 plots a time profile of the (M, N)-potential function defined in (1). One can see that it attained its minimum value (i.e., a desired phase state) for each coordination phase. Although the precision of the formation distance still needs to be improved, this flight has demonstrated a capability of the controllers designed in Section II to realize different coordination configurations.

V. CONCLUSION

This paper proposed a multi-agents coordination controller based on the decentralized virtual leader approach. The control design uses an idea of realizing a splay or synchronized phase distribution around a VL on a circle orbit. The proposed controller has been implemented on our fixed-wing UAV platforms, and a fully-autonomous coordinated flight of three UAVs has been achieved. In several flight tests, incoherent decisions between the UAVs occurred due to communication delay/failures. In order to avoid such consensus problems, a supervision function which monitors phase management states of the other UAVs should be added. A precision of the formation distance can be improved by synchronizing GPS data of all the UAVs and also by improving performance of the flight controller.

REFERENCES

[1] J.J. Acevedo, B.C. Arrue, I. Maza and A. Ollero, Cooperative Large Area Surveillance with a Team of Aerial Mobile Robots for Long Endurance Missions. Journal of Intelligent & Robotic Systems, 2012.

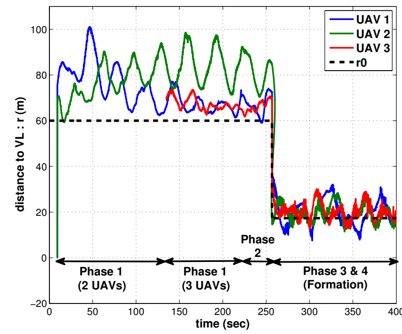

Fig. 7. Distance to Virtual Leader

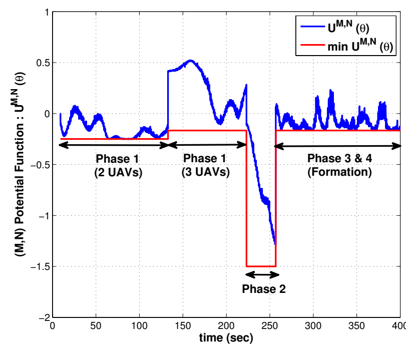

Fig. 8. (M, N)-Potential Function

[2] S. Hauert, J.C. Zufferey and D. Floreano, Reverse-engineering of Artificially Evolved Controllers for Swarms of Robots. IEEE Congress on Evolutionary Computation, 2009.

[3] A. Kushleyev, D. Mellinger and V. Kumar, Towards A Swarm of Agile Micro Quadrotors. Robotics: Science and Systems, 2012.

[4] Y.Q. Chen and Z. Wang, Formation Control : A review and A New Consideration. IEEE/RSJ International Conference on Intelligent Robots and Systems, 2005.

[5] E.N. Johnson, A.J. Calise, Y. Watanabe, J. Ha and J.C. Neidhoefer, Real-Time Vision-Based Relative Aircraft Navigation. AIAA Journal of Aerospace Computing, Information and Communication, 2007.

[6] Y. Gu, G. Campa, B. Seanor, S. Gururajan and M.R. Napolitano, Autonomous Formation Flight - Design and Experiments. Aerial Vehicles, Chapter 12, Intech, 2009.

[7] K.H. Tan and M.A. Lewis, Virtual Structures for High-Precision Cooperative Mobile Robotic Control. IEEE/RSJ International Conference on Intelligent Robots and Systems, 1996.

[8] W. Ren and R.W. Beard, Decentralized Scheme for Spacecraft Formation Flying via the Virtual Structure Approach. AIAA Journal of Guidance, Control and Dynamics, 2004.

[9] N.E. Leonard and E. Fiorelli, Virtual Leaders, Artificial Potentials and Coordinated Control of Groups. IEEE Conference on Decision and Control, 2001.

[10] T. Hino, Simple Formation Control Scheme Tolerant to Communication Failures for Small Unmanned Air Vehicles. International Congress of the Aeronautical Sciences, 2010.

[11] R. Sepulchre, D.A. Palay and N.E. Leonard, Stabilization of Planar Collective Motion: All-to-All Communication. IEEE Transactions on Automatic Control, 2007.

[12] H.K. Khalil, Nonlinear Systems. Prentice Hall Inc., 2002.

[13] Y. Watanabe, Coordinated Control of Multiple UAVs: Theory and Flight Experiment. AIAA Guidance, Navigation and Control Conference, 2013.